applied sciences

MDPI

Article

Study of the Compression Behavior of Steel-Fiber Reinforced Concrete by Means of the Response Surface Methodology

Ángel de la Rosa, Gonzalo Ruiz * and Elisa Poveda

ETS de Ingenieros de Caminos, C. y P., Universidad de Castilla-La Mancha, Av. Camilo José Cela s/n, 13071 Ciudad Real, Spain; Angel.delaRosa@uclm.es (Á.d.l.R.); Elisa.Poveda@uclm.es (E.P.)

* Correspondence: Gonzalo.Ruiz@uclm.es

Received: 28 October 2019; Accepted: 2 December 2019; Published: 6 December 2019

Abstract: The compression behavior of steel-fiber reinforced concrete (SFRC) has been addressed exhaustively in recent decades thereby highlighting a variety of differences with regard to the effect that the addition of fiber has on it. In this paper, a detailed study of the subject is developed for which a database has been created, which includes 197 tests performed on cylindrical concrete specimens with dimensions of 150 × 300 mm^2 (diameter × height). By means of the response surface methodology, we disclose the relationship that exists between the geometric parameters of the fiber (length, diameter, and aspect ratio), their amount (fraction in volume), and some matrix parameters (compression resistance and maximum size of coarse aggregate) with the different compression responses of the SFRC, which are strength, elastic modulus, critical deformation under maximum load, and the volumetric deformation work in the pre- and post-peak branch. Linear polynomial models are chosen to adjust each response with the defined factors, and said variables are studied in a dimensional and non-dimensional format. From the results obtained, it is verified how the inclusion of steel-fibers produces notable improvements in ductility and the energy absorption capacity of the concrete when significantly increasing the works of volumetric deformation in the pre- and post-peak branch with respect to the matrix without fibers. In addition, a new model is analyzed, which describes the stress–strain curve of the compression behavior of the SFRC based on the increase of ductility and energy absorption. This model is characterized by a softening branch subsequent to the peak load determined by means of the residual compressive strength, a parameter that corresponds to the value of the compressive stress associated with a strain equal to three times that of the peak of the curve, which is significantly dependent on the aspect ratio and fiber content.

Keywords: steel-fiber reinforced concrete (SFRC); compressive ductility; response surface methodology (RSM); compression behavior model of the SFRC; residual compressive strength

1. Introduction

The compression behavior of steel-fiber reinforced concrete (SFRC) has been widely addressed over the last four decades, as reflected in the extensive existing bibliography, which includes both experimental research, as well as analytical and numerical research. There is a variety of opinions with respect to the influence that the addition of steel-fiber has on such behavior, fundamentally in regards to resistance and stiffness. There is consensus on the increase of ductility and toughness that the material experiences.

As concerns the compressive strength, f_{cf}, we find works that indicate that the inclusion of steel-fibers in concrete involves from negligible [1,2] or marginal [3,4] increases to significant increases [5–8], although it is certain that the majority of authors contend that an improvement

occurs [3,5,8–23]. Nevertheless, others indicate that fibers do not contribute to the increase of the strength [24]. In addition, there is research that indicates that improvements may occur up to a certain value of the fiber content [19,25,26]. Among the reasons given for this variation in opinions are the effect of fibers on the transversal confinement of the specimens [14,15], the influence of the so-called fiber factor (product of the volumetric fiber ratio by its fiber aspect ratio, $\phi_f \lambda$) [27], the sensitivity to the fiber volume–aggregate size relationship, linked to the workability of the material [27], and the creation of additional voids in the concrete matrix [14,24].

In regard to the elasticity modulus, E_f, there also appears a disparity of results. There are works that demonstrate that the addition of steel-fibers tends to reduce it [13,14,28–30], while in others, an increase has been recorded [3,15–18]. The reasons for explaining the decrease are associated with the creation of additional voids that involve the inclusion of fibers [28–30].

With regard to the critical strain at peak load, ϵ_{cf}, there is a consensus that an increase occurs with the addition of steel-fibers [3,6,8,16–18,31–34], which is associated both with ϕ_f, as well as λ [14] and with the mentioned fiber factor [18,29]. The influence that the increase of f_{cf} [18,29,35,36] has on this parameter is also reported.

Once the maximum load is reached is when the principal effect of the steel-fibers is observed on the compression behavior of the concrete in terms of ductility and toughness. In all the works consulted, it is evident that the addition of fiber increases the capacity of energy absorption during the strain of the material, thereby improving its ductility [3–6,14–18,24,31–34,37–39]. This is due fundamentally to the greater effect of transversal confinement that fibers provide [5,6,14,15,18,24].

On the other hand, the design and analysis of the structural elements made with SFRC requires the application of models that are capable of representing with exactitude their mechanical behavior for purposes of being able to be included in the current design codes and structural requirements. In the scientific literature, there is a variety of models that, as a function of their own experimental data, pursue approaching the stress–strain response of the SFRC in compression [3,5,6,15,16,18,24,28,40]. With closer study, it may be verified how each one of them correctly adjusts to the data from which it comes; however, the adjustment is not as strong when they are subjected to the scrutiny of other experimental sources [30].

With this background, it is pertinent to propose a profound analysis for which the principal parameters are related to the concrete and steel-fibers that have an influence on the compression response of the SFRC. In particular, the increase of ductility and the capacity of energy absorption can be studied by means of the work of volumetric strain in the pre- and post-phases to peak load. For this purpose, a database has been created through an extensive bibliographic search in the scientific literature with compression results for SFRC. It includes a total of 197 uniaxial compression tests on cylindrical specimens with dimensions of 150×300 mm^2 (diameter $\times$ height) of SFRC with hook ended fibers with a single fold, in addition to their corresponding matrices without reinforcement. Subsequently, applying the response surface methodology [41], a series of factors, associated with the characteristics of the material (concrete matrix and fiber reinforcement), is analyzed, thereby identifying which have a great effect on the different responses of the compression strength for SFRC. Lastly, the compression stress–strain model for SFRC by Ruiz et al. [42] is studied. It permits the non-linear calculation of the structural elements of SFRC requested under compression that is based on the increase of ductility and energy absorption that the inclusion of steel-fibers provides to concrete.

2. Materials and Methods

2.1. Creation of the Database

Firstly, we proceed to the bibliographic search for publications with experimental results for uniaxial compressive tests on SFRC specimens (cylinders with dimensions of 150×300 mm^2, diameter $\times$ height, and steel-fibers with hooked-ends of a single fold), thereby creating a database with a total of 197 tests. The distribution of the number of tests collected for each one of the responses

to be studied is summarized in Table 1. Figure 1 shows the distribution of the data of the principal factors included in the database. Note that all the papers contributing to the database assume that the compressive behavior of the material is isotropic. This is so because the filling of this type of specimen does not lead to any preferential orientation of the fibers, since the fresh material does not flow along the form, nor pass through obstacles like narrow parts or bars.

Table 1. Database for uniaxial compression tests in steel-fiber reinforced concrete (SFRC) specimens.

	N° Specimens with Fibers	N° Specimens without Fibers
Compressive strength	167	30
Elastic modulus	83	17
Strain under maximum load	111	19
Volumetric deformation work before the peak load	90	14
Volumetric deformation work after the peak load	73	11

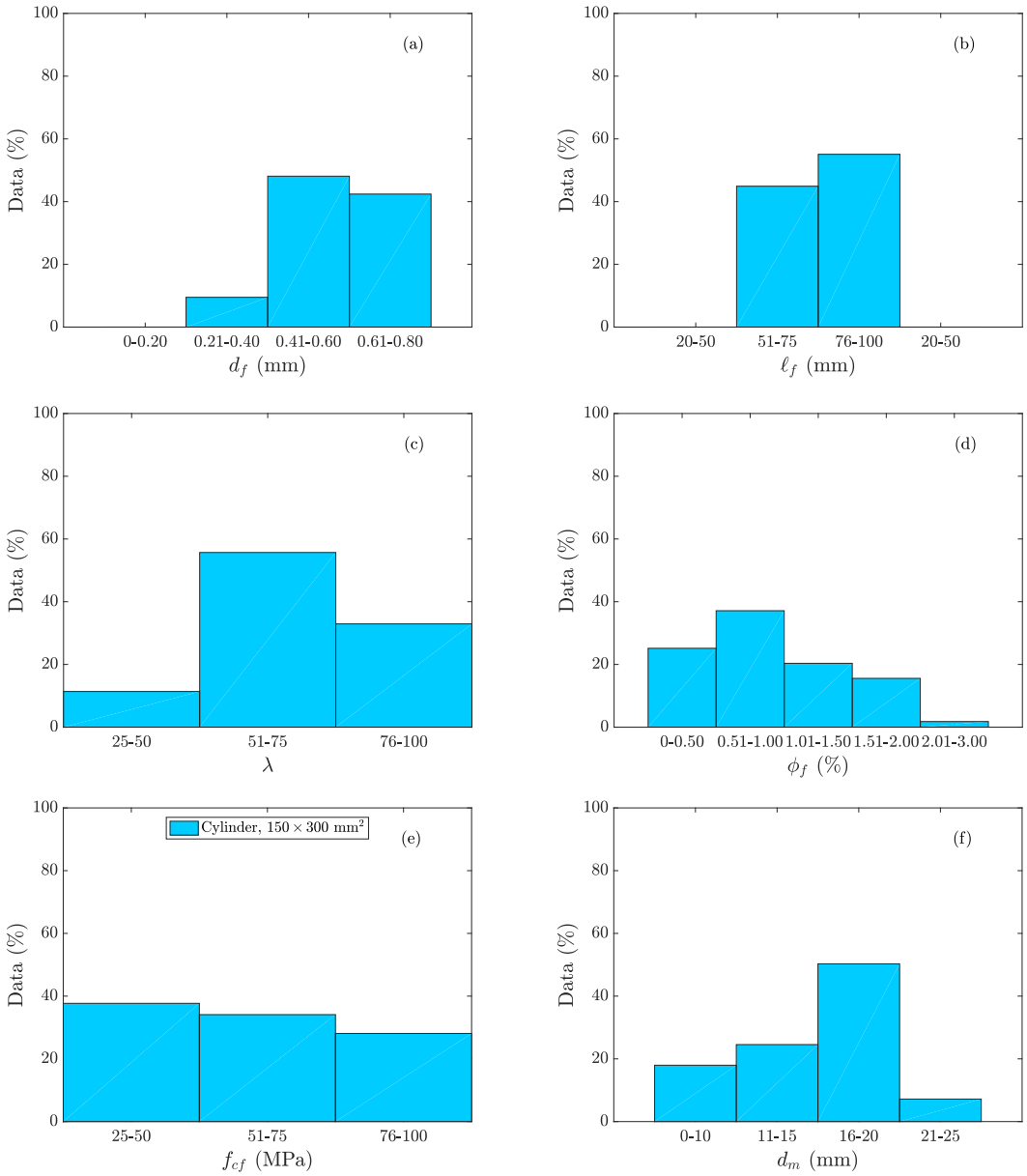

Figure 1. Distribution of the data of the principal factors included in the database: (**a**) diameter of steel-fiber, d_f; (**b**) fiber length, ℓ_f; (**c**) fiber aspect ratio, λ; (**d**) fiber content, ϕ_f; (**e**) compressive strength of SFRC, f_{cf}; and (**f**) maximum size of the coarse aggregate, d_m.

2.2. Response Surface Methodology

The response surface methodology (RSM) [41] consists of a collection of statistical-mathematical techniques applied to the creation of data adjustment models by means of which a series of parameters may be optimized and find the interactions that are produced between them [43,44]. It is a common method used in the improvement, development, and process management [45] in various industries, which has also been applied to those of concrete and cement for the design of mixtures [46–51], the analysis of resistant behavior [52–56], or the influence that the fiber content and the aspect ratio have in the optimization of the fracture of the fiber reinforced concrete [57].

This method permits the creation of regression adjustment models (by square minimums) of a set of data, as well as the optimization of a variable that is related to one or various dependent variables [58]. The analysis of the variance of the data (ANOVA) establishes the interaction between the variables for the purpose of estimating the statistical parameters and determining if there are significant relationships between the responses (dependent variables) and the factors (independent variables). By means of ANOVA, we verified the differences existing between the means of various populations, thereby seeking to separate how each source of variation contributes to the variation observed [59–61]. In addition, ANOVA must verify the normalcy of the populations in the distributions of the probability of the association between responses and factors, the equality of the variance of the populations, and the independence of the samples. If the ANOVA of a factor rejects the null hypothesis of the equality of averages, this signifies that there is a statistically significant association between the response and the factor, that is the response is influenced by the factor [59–61].

The RSM is based on the following steps: the statistical design and performance of experiments (or alternatively, as in our case, the formation of a database of experimental results) and the subsequent selection of the factors that may influence their responses, the choice of a suitable mathematical model or function to adjust the responses and the estimation of its parameters, the prediction of the responses, and the verification of the aptitude of the function in the experimental domain [43,62]. If there exists a continuous function, f, of the n factors that adjusts the actual values of the responses, then the response that corresponds to any set of factors can be written as:

$$y = f(x_1, x_2, \ldots, x_n) + \xi \quad (1)$$

where:

$f(x_1, x_2, \ldots, x_n)$: adjusted value of the response;
$x_1, x_2, \ldots, x_n$: independent variables or factors;
y: dependent variable or response;
ξ: error (arising principally from the experimental errors and adjustment [52]).

If f is not explicitly known, then it is necessary to find an adequate approximation in the correlation between factors and responses [43,63]. To do this, factors may be used to establish an empirical model correlated with the experimental data by means of a polynomial defined by Equation (2) [43]:

$$y = \beta_0 + \sum_{i=1}^{n} \beta_i x_i + \sum_{i=1}^{n} \beta_{ii} x_i^2 + \sum_{i=1}^{n-1} \sum_{j>i}^{n} \beta_{ij} x_i x_j + \xi \quad (2)$$

where:

β_0: independent term;
β_i: linear adjustment coefficients;
β_{ii}: quadratic adjustment coefficients;
β_{ij}: combined adjustment coefficients;

x_i, x_j: factors.

The experimental data that will be analyzed must belong to a family with a normal distribution function, which is presented through residues (the difference between the experimental values and the values obtained by the model adjustment). The normalcy of the residues indicates that the data distribution is normal as well [58]. The analysis was performed by means of the Minitab mathematical-statistical program [64].

2.2.1. Selection and Analysis of the Factors

The selection of the factors, with which the responses will be studied, is fundamental to achieve correct results. In addition, the data must proceed from quality sources and be within the ranges of observation sought for the responses. Thus, prior knowledge of the factors that affect the responses is a key aspect in the development of the procedure. For that reason, firstly, a selection has been made of a high number of factors that are considered to be able to have an influence on the compressive strength of the SFRC. Performing a first analysis in dimensional terms, both in the responses, as well as in the factors, a second analysis under the conditions of non-dimensionality is made for the purpose of observing, in addition to the statistical significance of the latter, the influence that they have on the variability of the responses. Lastly, a selection is made of the most significant factors obtained in the prior analysis with the objective of applying them to a simple model in a technological format that explains the uniaxial compression behavior of the SFRC [42]. Namely, they are the compressive strength of the base concrete, f_c, the maximum aggregate size, d_m, the diameter of the fiber, d_f, the length of the fiber, ℓ_f, the aspect ratio, λ, the fiber content, ϕ_f, and some combined parameters like the ratio between the length of the fiber and the maximum aggregate size, ℓ_f/d_m (note that the "Abbreviations" Section at the end of the paper gives a complete definition of all the symbols and acronyms used in this work).

2.2.2. Selection of the Response Model

Two regression adjustment models of the experimental data will be made, both polynomials, specifically first and second degree. The selection of the definitive model on which the work will be done, will be performed on the basis of the following criteria: its capacity to predict the response within the domain of the levels of the factors and especially adhering to the absence of multicollinearity. Multicollinearity is a problem that occurs when the explicative variables of the model are correlated among themselves. This gives rise to a reduction in the precision of the estimation of the coefficients of the terms of the factors, in addition to the possibility of concealing their statistical significance. An added difficulty for detecting the multi-collinearity is that it does not affect the goodness of the adjustment of the model. By means of the statistic variance inflation factor (VIF), the multicollinearity is studied. This index quantifies the severity of multicollinearity in an ordinary least squares regression analysis, since it measures how much the variance of an estimated regression coefficient is increased because of multicollinearity. It is calculated as:

$$\mathrm{VIF}(\hat{\beta}_j) = \frac{1}{1 - R_j^2} \tag{3}$$

where $\hat{\beta}_j$ is the value for the coefficient β_j estimated by the model and R_j^2 is its determination coefficient. If multicollinearity is severe, the variance of the determination coefficients is increased, which indicates that such coefficients are unstable, which in turn gives rise to false statistical factors' significances and erroneous values/signs of their coefficients. It is commonly accepted that if VIF > 5, then the multicollinearity is high [64,65].

Thus, VIF ≤ 5 was adopted as a limit for selecting the adjustment model, which is representative of a moderately low presence of multicollinearity, thereby deeming it very low or absent if VIF $\simeq 1$ [64].

2.2.3. Statistical Analysis of the Experimental Data

By means of ANOVA, statistics will be estimated, which will permit us to analyze the information of the database. The degree of statistical significance will be determined by means of the value of probability p (p-value) at the confidence interval of 95%. Thus, statistical significance is deemed to exist if the p-value ≤ 0.05. Concerning the study of factors, if the p-value calculated for a term is less than or equal to 0.05, there is a statistically significant relationship between said term and the response, thereby demonstrating that this effect is not due to randomness.

The adjusted determination coefficient R_a^2 indicates the goodness of the adjustment of the model. It is calculated with the following equation:

$$R_a^2 = 1 - \frac{N-1}{N-k-1}(1-R^2) \tag{4}$$

where k is the number of explanatory variables (or predictors) and R^2 is the standard determination coefficient, the formula of which is:

$$R^2 = \frac{\sum_{i=1}^{N}(\hat{y}_i - \bar{y})^2}{\sum_{i=1}^{N}(y_i - \bar{y})^2} \tag{5}$$

where N is the sample size or total number of observations; $\hat{y}_i$ is the estimated value for y in observation i according to the model; $\bar{y}$ is the mean value of y; and y_i is the actual value for y in observation i. R_a^2 concerns a more appropriate statistic than R^2 for verifying models with a different number of predictors since R^2 always increases when adding a new explanatory variable, even when there is not a real improvement in the model because such a factor is not relevant. R_a^2 corrects this overestimation, thereby reducing its value if an effect does not produce an improvement of the model [64].

2.3. Stress–Strain Model for the Uniaxial Compression Behavior of SFRC for Non-Linear Analysis

Ruiz et al. [42] developed a model, in a technological format, for the non-linear calculation of the compression behavior of the structural elements of SFRC. This model consists of two stress–strain curves: The first departs from the origin of the coordinates and reaches the maximum stress value and is analogous to the curve defined for plain concrete in Eurocode 2 [66] (Equation (6)). The second curve starts with maximum stress and manages to intercept the x-axis. This segment is defined by means of an inverted parabola of the vertical axis (Equation (7)), which has been calculated in such a way that the subsequent post-peak energy consumption is equal to the value of that same energy calculated in conformity with the data collected in the database. Figure 2 shows the stress–strain relationship, in reference to the SFRC and presented in a non-dimensional manner. The expression for the first curve (Stretch 1 in Figure 2) is:

$$\sigma^* = \frac{\alpha\,\epsilon^* - \epsilon^{*2}}{1 + (\alpha - 2)\,\epsilon^*} \tag{6}$$

where:

σ^*: non-dimensional stress ($\sigma^* = \frac{\sigma}{f_{cf}}$);
f_{cf}: compressive strength of the SFRC (cylinders 150 × 300 mm^2, diameter × height);
α: non-dimensional coefficient ($\alpha = 1.05\,\epsilon_{cf}\,\frac{E_f}{f_{cf}}$);
ϵ_{cf}: critical strain corresponding to f_{cf};
E_f: elastic modulus of SFRC;
ϵ^*: strain relative to the critical strain corresponding to f_{cf} ($\epsilon^* = \frac{\epsilon}{\epsilon_{cf}}$).

Note that the light blue area below curve 1 in Figure 2 is equal to $W_{1f}/f_{cf}\epsilon_{cf}$ ($= W_1^*$), which is the non-dimensional volumetric deformation work in the pre-peak branch relative to $f_{cf}\epsilon_{cf}$.

The second curve (Stretch 2 in Figure 2) can be expressed as:

$$\sigma^* = 1 - \frac{1}{4}\left(1 - \sigma_R^*\right)\left(\epsilon^* - 1\right)^2 \tag{7}$$

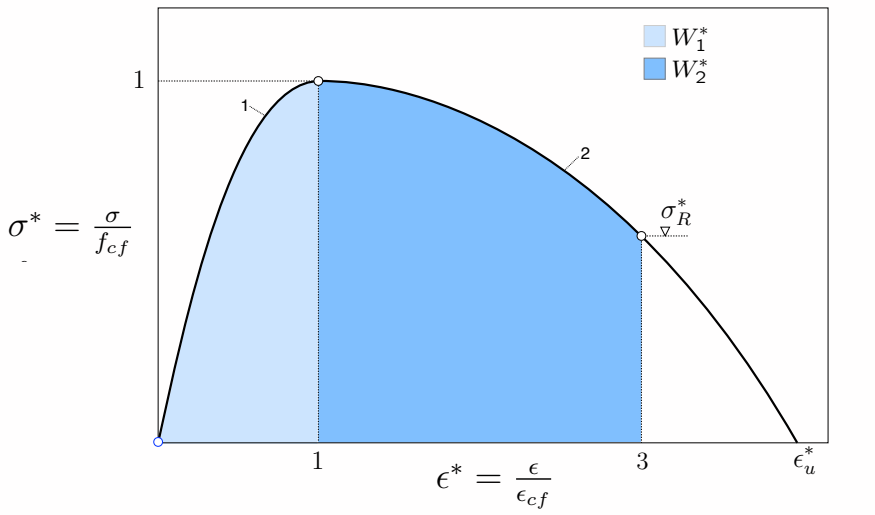

Figure 2. Non-dimensional stress–strain relationship in SFRC for structural analysis.

This softening branch of the model (Equation (7)) is determined by a parameter, σ_R^*, which is the residual compressive strength associated with $\epsilon^* = 3$ (Figure 2). It is defined so that the softening parabola consumes the same energy as the actual σ-ϵ curve between the peak and $3\,\epsilon_{cf}$. Therefore, the expression to obtain σ_R^* from an experimental σ-ϵ record is:

$$\sigma_R^* = \frac{3\,W_{2f}}{2\,f_{cf}\epsilon_{cf}} - 2 \tag{8}$$

where W_{2f} is the area below the σ-ϵ curve between ϵ_{cf} and $3\,\epsilon_{cf}$, that is the deformation work per unit volume consumed by the specimen from the peak of the curve to a strain three times larger than that of the peak. $W_{2f}/f_{cf}\epsilon_{cf}$ $(= W_2^*)$ is represented as the dark blue area in Figure 2. The reason for choosing σ_R as a reference is due to the fact that in all the tests included in the database that present diagrams of the σ-ϵ curves, at least this value is achieved; in other words, these specimens deformed and consumed energy up to $3\,\epsilon_{cf}$ at least. The softening curve in Equation (7) is on the safe side since the majority of the curves collected are capable of consuming more energy than that proposed in the model. In addition, σ_R^* is always less than the unit in such a way that the model does not take into consideration the possibility of having hardening due to compression deformation. In the case of seeking to consider it, the parabola could be replaced by a straight horizontal line ($\sigma_R^* = 1$), limiting the ultimate strain value, ϵ_u.

The model depends on two points: the value of the maximum compressive strength and its corresponding strain (f_{cf}, ϵ_{cf}) and the value of the stress associated with a strain three times greater than the critical and said strain (σ_R, $3\,\epsilon_{cf}$). In a non-dimensional manner (dividing the stresses by f_{cf} and the deformations by ϵ_{cf}) in the curve σ^*-ϵ^*, the defined points correspond to (1, 1) and (σ_R^*, 3), respectively. The equation that defines σ_R^* will be calculated by applying the RSM to the database as is subsequently seen. Both f_{cf}, as well as ϵ_{cf} and E_f may be measured with the uniaxial compression test [67]; however, they may also be explained by means of equations dependent on the fiber parameters. All this will be explained in greater detail in the subsequent section.

The most relevant aspect of the model of Ruiz et al. [42] is that it takes into account the capacity of energy absorption that the SFRC may reach after surpassing the maximum stress value (the area under the σ-ϵ curve represents the energy consumption by the unit of volume), which is notably greater than

that corresponding to its base concrete and is only being considered until a deformation value equal to $3\,\epsilon_{cf}$. As a consequence, the new σ^*-ϵ^* curve that is proposed permits considering the increase of the ductility that the inclusion of steel-fibers provides in SFRC structures.

Finally, it should be highlighted that this σ-ϵ curve assumes an isotropic behavior of the material. However, orientation factors similar to those used to modify the constitutive equations in tension [68,69] could be applied to adjust the proposed compressive σ-ϵ curve in case it were found that fiber orientation influences it. Vicente et al. [70] recently studied this topic using CT scanning to determine the orientation of fibers in concrete cubes that were later on tested in compression. They concluded that fiber orientation has a small impact on the compressive strength of concrete, although additional research could be done to determine whether it influences the ductility in compression or the residual compressive strength.

3. Results and Discussion

3.1. Responses of the Compression Behavior of the SFRC: Analysis with Physical Magnitudes

From the information of the database, the responses that describe the compressive strength of the SFRC, which are f_{cf}, E_f, ϵ_{cf}, W_{1f}, and W_{2f}, have been studied. Each one of them has been analyzed by means of the following factors: the compressive strength of the base concrete or matrix without fibers, f_c, the maximum size of the aggregate, d_m, the parameters that define the geometry of the fiber ℓ_f, d_f, and λ, the fiber volume ratio, ϕ_f, and a parameter that takes into account the relationship between the sizes of fiber and the aggregate, ℓ_f/d_m.

Figure 3 shows a scheme of the process followed to apply the RSM to the results from the database. All the responses were initially adjusted to two models of complete first and second degree polynomic regression. However, it was verified that the second degree models did not correctly predict the responses in the definition domain of the levels of the factors, for which reason they were disregarded for their use in the analysis. Furthermore, these models had excessively high VIF values in the majority of their terms, which indicated the presence of a strong multicollinearity. As stated above, this phenomenon caused the loss of precision in the estimation of the coefficients of the factors, as well as alterations in the detection of their statistical significance. It bears emphasizing that the fiber factor, $\phi_f\lambda$, was not found to be significant in the two degree polynomial models, neither in the quadratic nor in the combined adjustments, as shown in the Pareto diagrams in Figure 4. The corresponding VIFs were 3.85 and 2.85, respectively. Thus, it can be assumed that the level of multicollinearity for $\phi_f\lambda$ in both cases was low, and consequently, the low significances given by ANOVA were reliable.

Therefore, the analysis of the responses has been performed exclusively with first degree models (Equation (9)). After verifying that the linear models correctly predicted the responses in the domain of the definition of factors, the study of the VIF revealed that they were greater than 10 in the majority of factors, except for f_c and ϕ_f, for which VIF $\simeq 1$. This fact demonstrated that multicollinearity still existed, for which reason it would be appropriate to make a selection and reduce the number of factors with which the responses are analyzed.

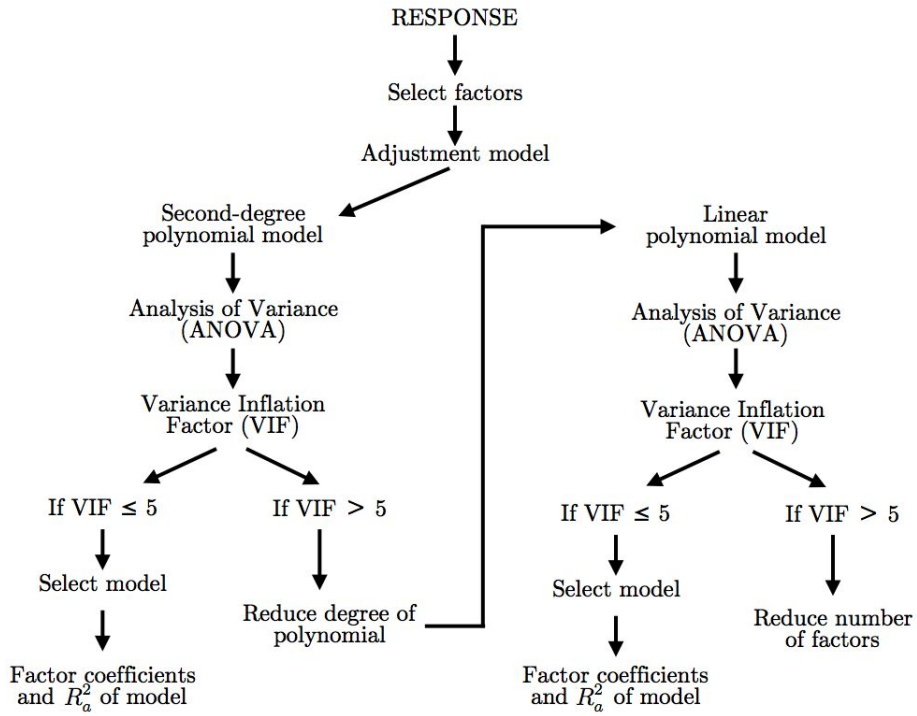

Figure 3. Diagram of the steps followed in the RSM calculation process.

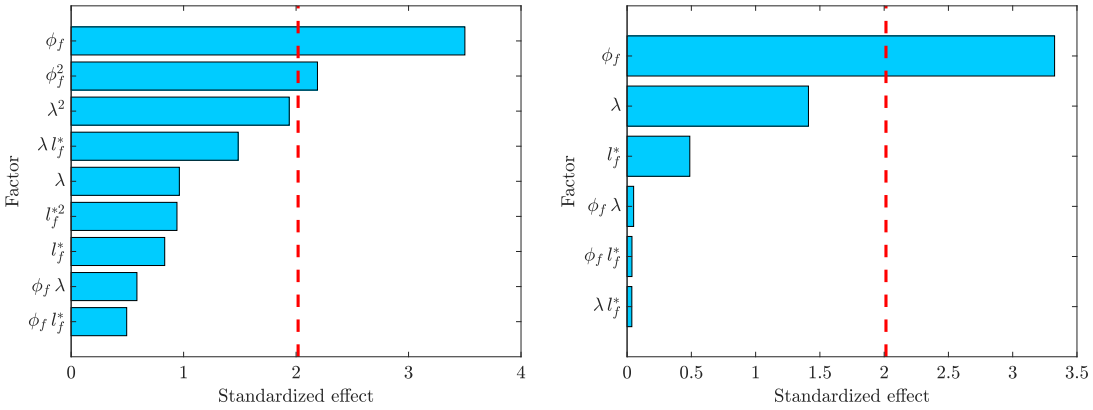

Figure 4. Pareto diagrams for the quadratic (**left**) and combined (**right**) adjustments of the residual compressive strength.

The factors that were statistically significant were determined by making use of the Pareto diagrams. Table 2 contains coefficients of the β_i adjustment of the x_i factors in the linear models for each one of the responses, as well as the terms that were statistically significant. Each response can be calculated as:

$$y = \beta_0 + \sum_{i=1}^{n} \beta_i x_i + \xi \tag{9}$$

When making an adjustment among the variables that have different units, as is the case, some of the coefficients of the β_i factors also require units to conserve the dimensional stability. Thus, the β_0 coefficients will have the corresponding response units (for example, for the response f_{cf}, β_0 is expressed in MPa, and for the ϵ_{cf} response, β_0 does not have any units). For the remaining β_i coefficients of the factors, the definition of their units is as follows: the numerator corresponds to the response unit, and the denominator corresponds to the unit of the factor to which it is associated (for example, for the E_f response, the β_2 coefficient, associated with the d_m factor, has GPa/mm as

a unit). Subsequently, a non-dimensional analysis of the variables will be performed so that the β_i coefficients will be expressed without units, which facilitates the manipulation of expressions.

Table 2. β_i adjustment coefficients of the x_i factors in the linear models with dimensional responses (bold = statistically significant).

	β_0	f_c (MPa)	d_m (mm)	ℓ_f (mm)	d_f (mm)	λ	ϕ_f	$\frac{\ell_f}{d_m}$	R_a^2 (%)
f_{cf} (MPa)	−18.4	**1.0573**	**0.989**	−0.107	−11.6	0.020	**194.5**	**3.59**	90.4
E_f (GPa)	16.5	**0.2590**	**−1.574**	−0.380	**67.2**	**0.408**	**−474**	**−6.09**	45.9
ϵ_{cf}	3894×10^{-6}	$\mathbf{-4 \times 10^{-6}}$	-15×10^{-6}	$\mathbf{41 \times 10^{-6}}$	$\mathbf{-322 \times 10^{-5}}$	-14×10^{-6}	$\mathbf{-1689 \times 10^{-5}}$	-129×10^{-6}	22.4
W_{1f} (GJ/m^3)	0.533	**0.001431**	**−0.00823**	**0.01323**	**−0.829**	$\mathbf{-557 \times 10^{-5}}$	**2.468**	**−0.02547**	72.1
W_{2f} (GJ/m^3)	3.085	-636×10^{-6}	**−0.0935**	**0.065**	**−2.59**	−0.0158	**17.63**	**−0.563**	70.2

The diagrams of the residues obtained in the analysis indicated that they were distributed randomly, thereby adhering to a function of normal probability (Figure 5 shows two of the diagrams, for the compressive strength and for the volumetric deformation work in the post-peak). This confirms the premise that the origin of the experimental data must demonstrate normality in its distribution. The value of the R_a^2 goodness adjustment coefficient was not so important insofar as the interest of this first analysis concerns the identification of the factors that really affect the variation of the response. These factors were different for each of the responses studied, although it was certain that a series of factors appeared that had an effect on the majority of them: f_c was statistically significant in all the responses, except in W_{2f}; d_m and ℓ_f/d_m were statistically significant in all except for ϵ_{cf}; d_m was not significant only in ϵ_{cf}. Nevertheless, it must be highlighted what happens with the f_c and ϕ_f factors, the latter of which had a statistical significance in all the responses (note that W_{2f} was not affected by the strength of the matrix, which seemed to make sense since this work corresponded to the post-crack branch of the matrix). In addition, both f_c and ϕ_f were the only factors with VIF $\simeq$ 1, which was symptomatic of the true nature of the problem, as may be verified when studying the variables of a non-dimensional manner.

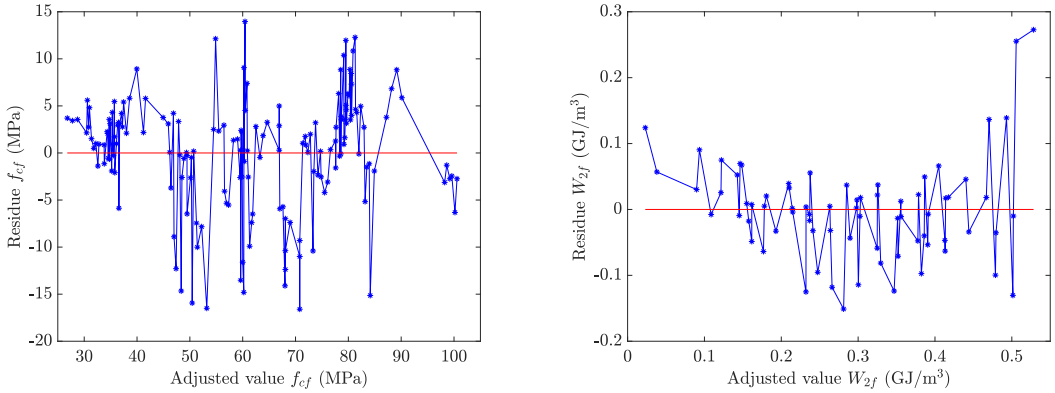

Figure 5. Residues of the compressive strength (f_{cf}, **left**) and the volumetric deformation work in the post-peak branch (W_{2f}, **right**).

3.2. Responses of the Compression Behavior of the SFRC: Non-Dimensional Analysis

Presented below are the results uncovered when applying the RSM in a non-dimensional manner. Each one of the responses and factors was divided by a parameter that had the same physical dimension: the responses were divided by the value of the same variable corresponding to the concrete matrix without fibers from which it proceeded (for example, the f_c° response resulted from the division of f_{cf} by f_c). Some factors with dimensions of length were divided by an auxiliary parameter, ℓ_0, which was the average value of the fiber lengths included in the database, which was roughly equal to 30 mm. The analysis of the f_c factor was eliminated from the analysis since it was actually present in the non-dimensional stresses. Besides, we sought to only study the influence of those factors that were

related to the materials (coarse aggregate and fiber) and not with the strength of the matrix (in the previous section, the statistical significance of f_c was verified in each one of the responses except in W_{2f}).

The objective that was pursued with this analysis was two-fold: on the one hand, to observe how each one of the factors affected the increase or the decrease of the responses and, on the other hand, to identify those factors that had a statistical significance that may be used in the proposed model, which describes the compression strength of the SFRC [42]. The responses were adjusted by means of the linear model. Table 3 presents the linear coefficients of the β_i adjustment of the x_i factors for each one of the responses (all are expressed in a non-dimensional form).

Table 3. Coefficients of β_i adjustment of the x_i factors in the linear models with non-dimensional responses (bold = statistically significant).

	β_0	$\frac{d_m}{\ell_0}$	$\frac{\ell_f}{\ell_0}$	$\frac{d_f}{\ell_0}$	λ	ϕ_f	$\frac{\ell_f}{d_m}$	R_a^2 (%)
f_c°	1	0.259	**0.1176**	**−11.65**	−0.00178	**3.75**	0.0223	10.7
E_c°	—	—	—	—	—	—	—	—
ϵ_c°	1	0.254	−0.0089	−3.35	−0.00261	**−13.94**	0.0363	40.0
W_1°	1	**−1.889**	**0.437**	19.1	0.0085	**48.62**	−0.253	35.2
W_2°	0.98	−3.13	0.99	−13	0.0375	**110.8**	−0.58	54.3

From this analysis, it follows that E_c° did not have a significant relationship with any factor. This result was in line with that demonstrated by the scientific literature regarding the disparity of conclusions concerning the effect that the addition of fiber has on the variability of the elastic modulus.

Once again, as a consequence of the number of factors that were introduced in the analysis, the VIFs obtained were higher in some terms (only ϕ_f maintained a VIF $\simeq 5$, as occurred in variables with dimensions). This fact may conceal factors that are significant and that do not appear as such and vice versa. For this reason, there will be a reduction in the number of factors to study in the compression behavior model of SFRC proposed by Ruiz et al. [42]. Three parameters: ℓ_f^*, λ, and ϕ_f, characteristic of fiber reinforcement and expressed in a non-dimensional manner, were selected. The reason for this choice was that the first two defined the geometry of the fiber and the last made reference to its content. In addition, ϕ_f was the only factor that had a statistical significance in each of the responses, and ℓ_f^* was the next factor with greater significance for all of them. On the other hand, these three parameters were those that intervened in the majority of the models existing in the literature that describes the σ-ϵ compression response of SFRC.

3.3. Stress–Strain Model of the Compression Response for SFRC

This section will study the influence that the factors ℓ_f^*, λ, and ϕ_f had on the SFRC compression model proposed by Ruiz et al. [42]. The most important aspect that must be highlighted is the gain in the capacity of energy absorption that the addition of steel-fibers in the concrete provides. It may increase up to 45% in the segment prior to the peak load and reach almost three times more in the segment subsequent to the peak load in average values with respect to the concrete without fiber reinforcement. In addition, once the maximum load has been surpassed, W_{2f} may reach a maximum value five times greater than the matrix without fiber. This fact demonstrates the increase in ductility that a structural element of SFRC, requested at uniaxial compression, may exhibit. Table 4 shows the statistical values of each one of the analyzed responses of the compression strength of SFRC obtained from the tests included in the database.

From the linear adjustment and the statistical analysis of the relationships between the defined variables, the β_i coefficients of the model were calculated. They are included in Table 5. Figures 6–9 represent the Pareto diagrams for the f_c°, ϵ_c°, W_1°, and W_2° responses, as well as the adjustment diagrams of their response surfaces with respect to the statistically significant factors.

Table 4. Statistics of the responses of the parameters of the σ-ϵ model for SFRC proposed by Ruiz et al. [42].

	Mean	**(Std. dev.)**	**[Max.–Min.]**
f_c°	1.04	(0.12)	[0.69–1.34]
E_c°	0.99	(0.08)	[0.76–1.21]
ϵ_c°	1.27	(0.30)	[0.93–2.51]
W_1°	1.45	(0.52)	[0.91–3.73]
W_2°	2.83	(1.09)	[1.12–5.49]

Table 5. β_i adjustment coefficients of the x_i factors and the non-dimensional responses, calculated for the σ-ϵ model for SFRC proposed by Ruiz et al. [42] (bold = statistically significant).

	$\boldsymbol{\beta_0}$	$\boldsymbol{\ell_f^*}$	$\boldsymbol{\lambda}$	$\boldsymbol{\phi_f}$	$\boldsymbol{R_a^2}$ **(%)**	**VIF**
f_c°	0.980	0.0151	189×10^{-6}	**2.94**	5.3	[1.3–5.3]
E_c°	—	—	—	—	—	—
ϵ_c°	0.996	$\mathbf{-0.0959}$	$\mathbf{185 \times 10^{-5}}$	**28.23**	36.1	[1.5–2.1]
W_1°	0.929	0.143	-251×10^{-5}	**40.97**	31.6	[1.3–5.1]
W_2°	0.770	−0.048	$\mathbf{1444 \times 10^{-5}}$	**96.90**	50.8	[1.6–4.6]
σ_R^*	−0.131	−0.0717	$\mathbf{609 \times 10^{-5}}$	**21.72**	29.7	[1.0–1.7]

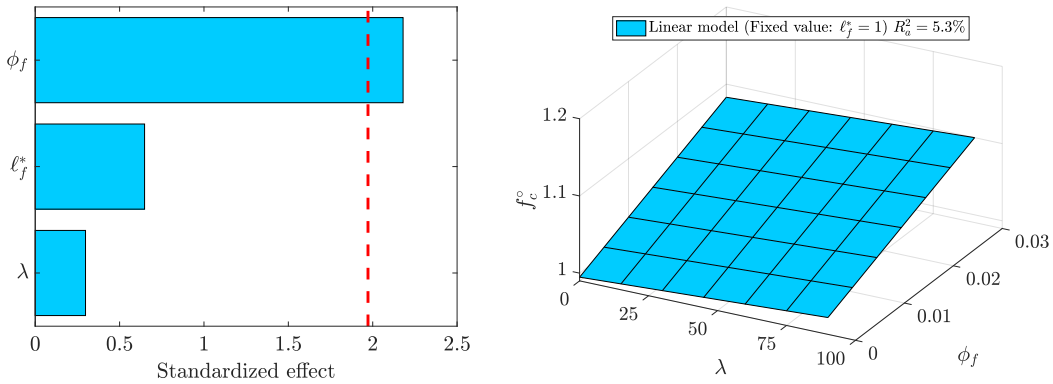

Figure 6. Pareto diagram and response surface of f_c°.

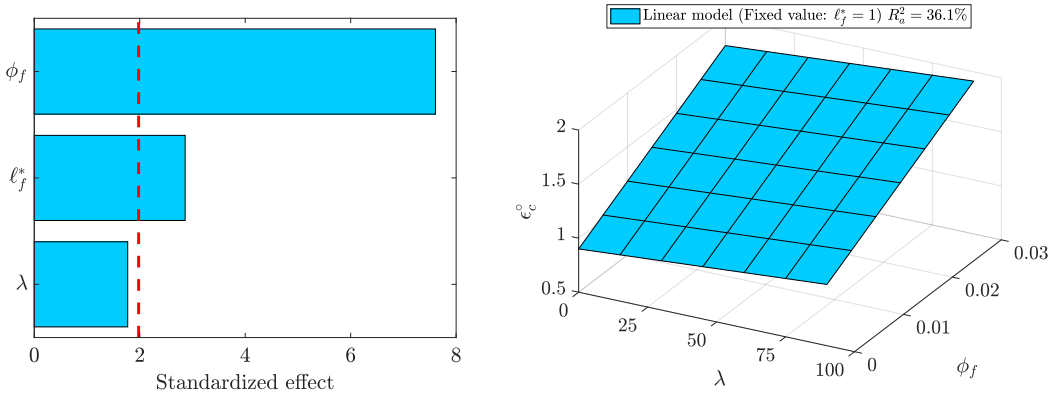

Figure 7. Pareto diagram and response surface of ϵ_c°.

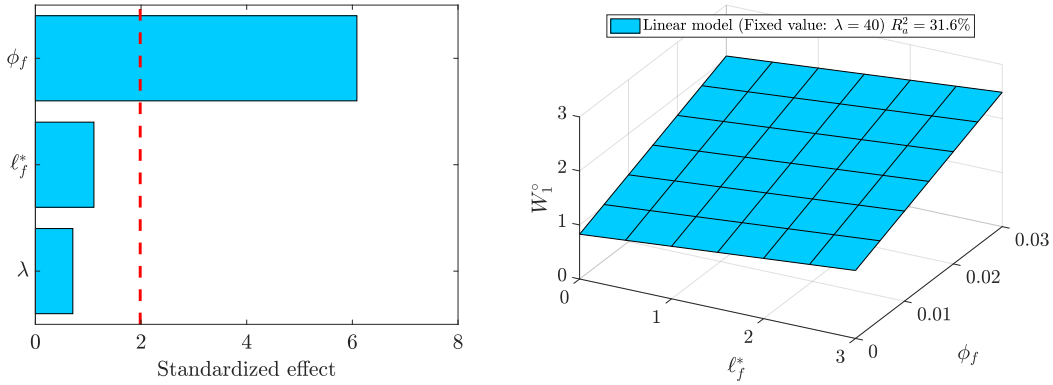

Figure 8. Pareto diagram and response surface of W_1°.

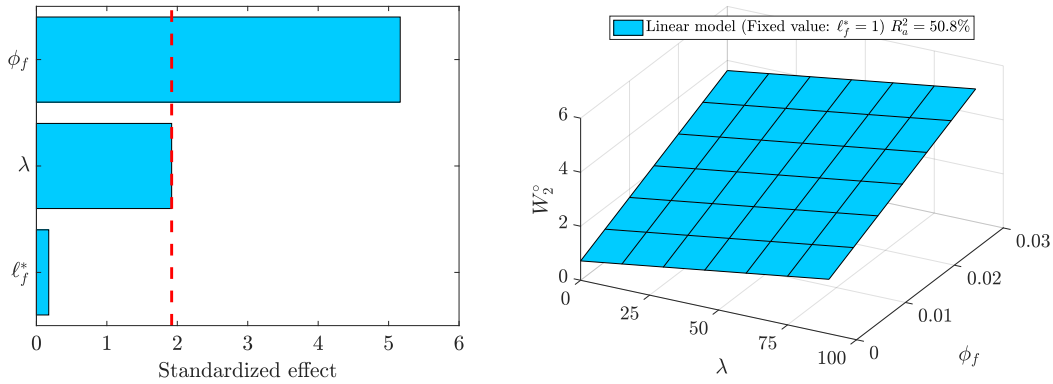

Figure 9. Pareto diagram and response surface of W_2°.

Once again, the absence of the statistically significant relationship of E_c° with any factor was verified, as occurred in the prior analysis, which included a majority of factors in the model, thereby reinforcing the idea of the absence of the relationship between the variability of the elasticity modulus and the inclusion of the fiber in the concrete. The physical reason behind this fact maybe that, as the fiber content increases, the SFRC porosity also increases, which in turn leads to a decrease in the modulus of the base concrete that compensates the stiffening effect due to the presence of fibers.

Insofar as f_c°, the SFRC compression strength, it was only significantly affected by ϕ_f, thereby demonstrating a slight increase as fiber was added. Despite the low value of R_a^2 (5.3%), the statistical significance, demonstrated by ϕ_f, and the positive value of its adjustment coefficient in the model indicated the tendency of the increase of f_c°, in mean values. This is how this effect must be interpreted, as observed in Figure 10. The value of f_c° may be easily measured through the uniaxial strength test [67] or calculated by means of Equation (10), which was obtained from a new linear correlation between f_c° and ϕ_f alone:

$$f_c^\circ = 1 + 3.80\,\phi_f \quad (R_a^2 = 4.5\%) \tag{10}$$

The RSM can also provide the characteristic value, understood as the value corresponding to a cumulative probability of 5% in the distribution curves, as shown in Figure 10. The result is:

$$f_{ck}^\circ = 0.825 + 3.75\,\phi_f \tag{11}$$

Furthermore, ϵ_c° may be experimentally measured with the uniaxial compression test, although it also may be estimated with the coefficients of Table 5.

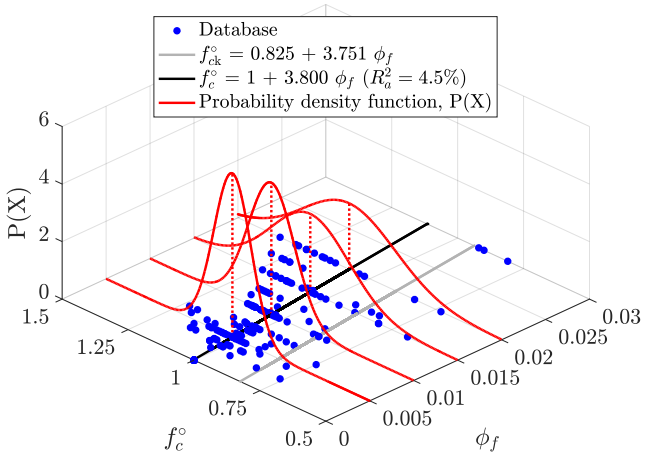

Figure 10. Linear adjustment with the average and characteristic values of f_c°.

The residual compressive strength, σ_R^*, defined in the model of Ruiz et al. [42] (equal to the non-dimensional compressive stress associated with a deformation $\epsilon^* = 3$) is calculated in Equation (12):

$$\sigma_R^* = -0.131 + 21.72\,\phi_f + 0.00609\,\lambda - 0.0717\,\ell_f^* \quad (R_a^2 = 29.7\%) \tag{12}$$

In the analysis performed, ϕ_f and λ were statistically significant, for which reason a new analysis was executed again with the result that both of these factors were once again significant. ϕ_f and λ were then related to σ_R^* by means of Equation (13):

$$\sigma_R^* = -0.089 + 21.27\,\phi_f + 0.00407\,\lambda \quad (R_a^2 = 21.3\%) \tag{13}$$

Figure 11 represents the Pareto diagram and the response surface of the statistically significant factors of σ_R^*. Its corresponding characteristic value is:

$$\sigma_{R\mathrm{k}}^* = -0.389 + 21.14\,\phi_f + 0.00422\,\lambda \tag{14}$$

It should be noted that Equations (13) and (14) are defined only for concretes with a minimum fiber content and thus, they do not provide negative values (indeed, all the SFRCs in the database yielded positive residual strengths since the minimum values in the database for ϕ_f and λ were 0.0024 and 20, respectively). It should be reminded that σ_R^* can also be obtained from experimental σ-ϵ records using Equation (8). It bears emphasizing that both f_c° and σ_R^* were calculated in mean values since the database contained exclusively the tests' results. Nevertheless, in light of the concept of characteristic resistance (expressed as that corresponding to the quantile of 5% in the distribution of resistances obtained in a group of tests on similar specimens), Equations (11) and (14) were determined. They permit calculating the characteristic values of f_c° and σ_R^*, if one wishes to work with them.

The residual compressive strength can also be related to the residual flexural strengths $f_{R,1\mathrm{k}}$ and $f_{R,3\mathrm{k}}$, which are the flexural strengths for crack mouth opening displacements of 0.5 mm and 2.5 mm. Ruiz et al. [71] showed that the dimensional and non-dimensional expressions relating these parameters, on average and in characteristic fashion, are:

$$\sigma_R = -1.77 + 1.807\,f_{R,1\mathrm{k}} + 9.12\,\frac{f_{R,3\mathrm{k}}}{f_{R,1\mathrm{k}}} \tag{15}$$

$$\sigma_R^* = 0.1839 + 0.02203\,f_{R,1\mathrm{k}} \tag{16}$$

$$\sigma_{R\mathrm{k}} = -7.6205 + 1.79989\,f_{R,1\mathrm{k}} + 9.1151\,\frac{f_{R,3\mathrm{k}}}{f_{R,1\mathrm{k}}} \tag{17}$$

$$\sigma^*_{Rk} = 0.1094 + 0.02190\, f_{R,1k} \quad (18)$$

The residual flexural strengths $f_{R,1k}$ and $f_{R,3k}$ in Equations (15)–(18) were introduced in MPa; the residual compression strengths σ_R and σ_{Rk} were obtained in MPa, whereas σ^*_R and σ^*_{Rk} were non-dimensional. Equations (15)–(18) were derived from an RSM study on a flexural database with experiments reported by Tiberti et al. [72]. Note that non-dimensional values of the residual compressive strength depended only on $f_{R,1k}$ because the ratio $f_{R,3k}/f_{R,1k}$ was not found to be significant for them [71]. It bears emphasizing that fibers greatly enhanced both flexural and compressive SFRC behavior as compared with the same values of the corresponding base concrete. However, so far, it was only the flexural behavior of SFRC that was accounted for by the standards in [68,69], to the extent that the characteristic residual flexural strengths $f_{R,1k}$ and $f_{R,3k}$ were taken as indices to perform an SFRC classification [69]. Consequently, as stated in [71], it is appropriate to relate the residual compressive strength σ_R to its flexural counterparts, not only to the fiber parameters.

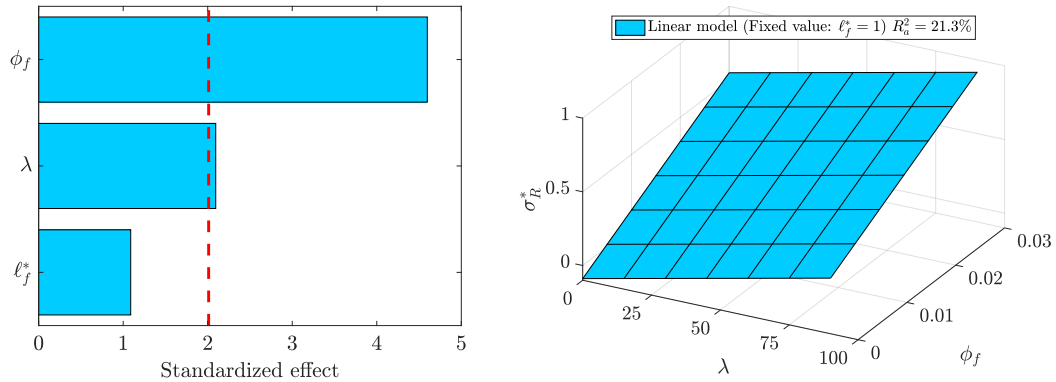

Figure 11. Pareto diagram and response surface of σ^*_R.

In the responses ϵ°_c, W°_1, W°_2, and σ^*_R, the ϕ_f factor was statistically significant, and its effect was positive on their variation. λ was also significant on ϵ°_c, W°_2, and σ^*_R with a positive effect on variability. This demonstrated that the ductility and capacity of energy absorption from the maximum strength in the phase subsequent to the cracking of the SFRC were governed by a parameter related to the geometry of the fiber, such as λ, and for the fiber content, ϕ_f. This result was in line with that set forth by Shah et al. [31,32] for SFRC and by Fanella et al. [31,33] for steel-fiber reinforced mortars. As previously explained, the importance of the statistical analysis lies with the determination of the significance of the factors and not with the R^2_a goodness adjustment coefficient since this permits determining if a factor has a real influence on the explanation of the response variability. The coefficients R^2_a only indicated the dispersion of the data around the mean adjustment surface of the selected linear model. Finally, it must be emphasized that the VIF statistic had a value ≤ 5 in almost all of the analyzed responses. Actually, the VIF reached a maximum value of 5.3, which may be accepted in terms of the moderately low multicollinearity in the statistical analysis of the model that was performed.

4. Conclusions

This article studied the influence that a series of parameters, related to the concrete matrix and reinforcement of fiber, have on the compression behavior of SFRC. By means of an extensive search of the scientific literature, a database was compiled, which included a total of 197 uniaxial compression tests performed on 150 × 300 mm^2 (diameter × height) cylinders. The database included the results of experimental campaigns developed with steel-fiber reinforced concrete with hooked end fibers and a single fold and their respective matrices without steel-fiber reinforcement. The data analysis was performed by means of the response surface methodology, which consisted of a set of statistical and mathematical techniques applied to the creation of data adjustment models, which enabled the optimization of parameters and the search for the interactions that occurred between them. The study

was done with first and second degree polynomic adjustment models. The latter was eliminated for not correctly predicting the responses in the domain of the definition of the factors and for presenting strong multicollinearity.

Firstly, the descriptive variables of the compression response of the SFRC (f_{cf}, E_{cf}, ϵ_{cf}, W_{1f}, and W_{2f}) were selected and correlated with factors associated with the matrix without reinforcement (f_c and d_m), with factors that define the geometry of the fiber (ℓ_f, d_f, and λ), with its content (ϕ_f), and the relationship between the sizes of the fiber and aggregate (ℓ_f/d_m). From the analysis performed, it was found that ϕ_f was statistically significant for all the responses and that f_c was also significant, except for W_{2f}, which corresponded to the work on post-crack volumetric deformation. In addition, both of them were the only factors in which multicollinearity was not present. The so-called fiber factor, $\phi_f\lambda$, was not found to be significant.

Subsequently, the responses and factors were analyzed in a non-dimensional manner. Only the fiber content, ϕ_f, was significant for all the responses and demonstrated moderate multicollinearity. The fiber length, ℓ_f, was the next factor that was shown to have a great influence on responses. Both factors, together with the aspect ratio, λ, were chosen to analyze the compressive strength model of the SFRC of Ruiz et al. [42] (it dealt with representative parameters of the geometry and fiber content, used in the majority of the models applied to the SFRC). The proposed model considered the increase of ductility and the energy absorption that the inclusion of fiber to the concrete provided. In particular, its curve, σ-ϵ, referring to the concrete with fibers, in the softening branch was calculated in such a manner that the subsequent consumption of energy after peak load was equal to the value of that same energy calculated in conformity with the data collected in the database. This softening branch was defined by a parameter, σ_R, which was the compressive residual strength associated with $\epsilon = 3\,\epsilon_{cf}$. The factor ϕ_f was statistically significant in all the responses, and λ was also in ϵ_{cf}, W_{2f} and σ_R. This fact demonstrated that the ductility and the capacity of energy absorption from the maximum stress in the post-cracking phase of the SFRC was governed by the geometry of the fiber through the aspect ratio λ and by its content ϕ_f.

Author Contributions: Conceptualization, Á.d.l.R. and G.R.; methodology, Á.d.l.R. and G.R.; software, Á.d.l.R.; validation, Á.d.l.R., G.R., and E.P.; writing, original draft preparation, Á.d.l.R.; writing, review and editing, G.R. and E.P.

Funding: The authors gratefully acknowledge the funding received from Ministerio de Ciencia, Innovación y Universidades, Spain, through Projects BIA2015-68678-C2-1-R and RTC-2017-6736-3. A.R. acknowledges the economic aid received by means of the grant FPI BES-2016-077458.

Conflicts of Interest: The authors declare no conflict of interest.

Abbreviations

The following abbreviations and nomenclature are used in this manuscript:

d_f	Diameter of steel-fiber
d_m	Maximum size of coarse aggregate
E_c	Elastic modulus of unreinforced concrete matrix in 150×300 mm^2 cylinders
E_s	Elastic modulus of steel
E_f	Elastic modulus of SFRC in 150×300 mm^2 cylinders
$E_c^\circ = \frac{E_f}{E_c}$	Non-dimensional elastic modulus of SFRC
f	Mathematical function
f_c	Compressive strength of unreinforced concrete matrix in 150×300 mm^2 cylinders
f_{cf}	Compressive strength of SFRC in 150×300 mm^2 cylinders
$f_c^\circ = \frac{f_{cf}}{f_c}$	Non-dimensional compressive strength of SFRC
$f_{R,1k}$	Characteristic residual flexural strength for $w_M = 0.5$ mm of SFRC in $150 \times 150 \times 550$ mm^3 prisms
$f_{R,3k}$	Characteristic residual flexural strength for $w_M = 2.5$ mm of SFRC in $150 \times 150 \times 550$ mm^3 prisms

i, j	Index assigned to factors and responses
k	Number of explanatory variables in an RSM adjustment
ℓ_f	Fiber length
$\ell_0 = 30\,\text{mm}$	Coefficient to keep non-dimensionality
$\ell_f^* = \frac{\ell_f}{\ell_0}$	Non-dimensional fiber length
n	Number of factors or independent variables
p-value	Statistical parameter to determine statistical significance
R^2	Determination coefficient/multiple correlation coefficient
R_a^2	Adjusted determination coefficient
R_j^2	Determination coefficient corresponding to estimate $\hat{\beta}_j$
RSM	Response surface methodology
SFRC	Steel-fiber reinforced concrete
VIF	Variance inflation factor
$W_1 = \int_0^{\epsilon_c} \sigma d\epsilon$	Volumetric deformation work in the pre-peak branch of unreinforced concrete matrix in 150×300 mm^2 cylinders
$W_{1f} = \int_0^{\epsilon_{cf}} \sigma d\epsilon$	Volumetric deformation work in pre-peak branch of SFRC in 150×300 mm^2 cylinders
$W_2 = \int_{\epsilon_c}^{3\epsilon_c} \sigma d\epsilon$	Volumetric deformation work in post-peak branch of unreinforced concrete matrix in 150×300 mm^2 cylinders
$W_{2f} = \int_{\epsilon_{cf}}^{3\epsilon_{cf}} \sigma d\epsilon$	Volumetric deformation work in post-peak branch of SFRC in 150×300 mm^2 cylinders
$W_1^* = W_{1f}/f_{cf}\epsilon_{cf}$	Non-dimensional volumetric deformation work in pre-peak branch of SFRC relative to $f_{cf}\epsilon_{cf}$
$W_2^* = W_{2f}/f_{cf}\epsilon_{cf}$	Non-dimensional volumetric deformation work in post-peak branch of SFRC relative to $f_{cf}\epsilon_{cf}$
$W_1^\circ = W_{1f}/W_1$	Non-dimensional volumetric deformation work in pre-peak branch of SFRC relative to W_1
$W_2^\circ = W_{2f}/W_1$	Non-dimensional volumetric deformation work in post-peak branch of SFRC to relative to W_1
w_M	Crack mouth opening displacement
x_i, x_j	Factors or independent variables
y	Response or dependent variable
$\bar{y}$	Mean value of y
$\hat{y}_i$	Estimated value for y in observation i
y_i	Actual value for y in observation i
α	Non-dimensional coefficient
β_0	Adjusted constant
β_i	Adjusted coefficient for a linear term
β_{ii}	Adjusted coefficient for a quadratic term
β_{ij}	Adjusted coefficient for a combined term
$\hat{\beta}_j$	Value for the coefficient β_j estimated by the RSM model to obtain the VIF
ϵ	Strain
ϵ_{cf}	Critical strain at peak load of SFRC in 150×300 mm^2 cylinders
ϵ_c	Critical strain at peak load of unreinforced concrete matrix in 150×300 mm^2 cylinders
$\epsilon^* = \frac{\epsilon}{\epsilon_{cf}}$	Strain relative to the critical strain at peak load of SFRC
$\epsilon_c^\circ = \frac{\epsilon_{cf}}{\epsilon_c}$	Critical strain at peak load of SFRC relative to the critical strain of the corresponding unreinforced matrix
ϵ_u	Ultimate strain of SFRC in 150×300 mm^2 cylinders
$\lambda = \frac{\ell_f}{d_f}$	Fiber aspect ratio
ξ	Error observed in the response
σ	Stress
σ_R	Compressive residual strength; $\sigma(3\,\epsilon_{cf})$
$\sigma^* = \frac{\sigma}{f_{cf}}$	Non-dimensional stress
$\sigma_R^* = \frac{\sigma_R}{f_{cf}}$	Non-dimensional compressive residual strength; $\sigma^*(3)$
ϕ_f	Volumetric fiber ratio (steel-fiber volume per m^3)

References

1. Köksal, F.F.; Altun, F.; Yigit, I.; Sahin, Y. Combined effect of silica fume and steel-fiber on the mechanical properties of high strength concretes. *Constr. Build. Mater.* **2008**, *22*, 1874–1880. [CrossRef]
2. *ACI 544.4R-96 State of the Art Report on Fiber Reinforced Concrete*; ACI: Farmington Hills, MI, USA, 2002.
3. Tasdemir, M.A.; Ilki, A.; Yerlikaya, M. Mechanical behaviour of steel fibre reinforced concrete used in hydraulic structures. In Proceedings of the International Conference of Hydropower and Dams, HYDRO 2002, Antalya, Turkey, 4–7 October 2002; pp. 159–166.
4. Bayramov, F.; Tasdemir, M.A.; Ilki, A.; Yerlikaya, M. Steel fibre reinforced concrete for heavy traffic load conditions. In Proceedings of the 9th International Symposium on Concrete Roads, Istambul, Turkey, 3–6 April 2004; pp. 73–82.
5. Williamson, G.R. The effect of steel-fibers on the compressive strength of concrete. In *SP–44: Fiber Reinforced Concrete*; ACI: Detroit, MI, USA, 1974; pp. 195–207.
6. Hsu, L.S.; Hsu, C.T. Complete stress–strain behavior of high–strength concrete under compression. *Mag. Concr. Res.* **1994**, *46*, 301–312. [CrossRef]
7. Lee, S.C.; Oh, J.H.; Cho, J.Y. Compressive behavior of fiber–reinforced concrete with end–hooked steel-fibers. *Materials* **2015**, *8*, 1442. [CrossRef] [PubMed]
8. Ezeldin, A.S.; Balaguru, P.N. Normal and high strength fiber reinforced concrete under compression. *J. Mater. Civ. Eng.* **1992**, *4*, 415–429. [CrossRef]
9. Johnston, C.D. Steel fibre reinforced mortar and concrete—A review of mechanical properties. In *Fiber Reinforced Concrete*; ACI: Detroit, MI, USA, 1974; pp. 127–142.
10. Dixon, J.; Mayfield, B. Concrete reinforced with fibrous wire. *J. Concr. Soc.* **1971**, *98*, 73–76.
11. Kar, N.J.; Pal, A.K. Strength of fiber reinforced concrete. *J. Struct. Div.* **1972**, *98*, 1053–1068.
12. Chen, W.; Carson, J.L. Stress–strain properties of randon wire reinforced concrete. *ACI J.* **1971**, *68*, 933–936.
13. Hsu, L.S.; Hsu, C.T. Stress–strain behavior of steel–fiber high–strength concrete under compression. *ACI Struct. J.* **1994**, *91*, 448–457.
14. Someh, A.K.; Saeki, N. Prediction for the stress–strain curve of steel-fiber reinforced concrete. *Proc. Jpn. Concr. Inst.* **1994**, *18*, 1149–1154.
15. Mansur, M.A.; Chin, M.S.; Wee, T.H. Stress–strain relationship of high–strength fiber concrete in compression. *ASCE J. Mater. Civ. Eng.* **1999**, *11*, 21–29. [CrossRef]
16. Nataraja, M.; Dhang, N.; Gupta, A. Stress–strain curves for steel–fiber reinforced concrete under compression. *Cem. Concr. Compos.* **1999**, *21*, 383–390. [CrossRef]
17. Neves, R.D.; Fernandes de Almeida, J.C.O. Compressive behaviour of steel fibre reinforced concrete. *Struct. Concr.* **2005**, *6*, 1–8. [CrossRef]
18. Barros, J.A.O.; Figueiras, J.A. Flexural behavior of SFRC: testing and modeling. *J. Mater. Civ. Eng.* **1999**, *11*, 331–339. [CrossRef]
19. Soroushian, P.; Lee, C.D. Distribution and orientation of fibers in steel-fiber reinforced concrete. *ACI Mater. J.* **1990**, *87*, 433–439.
20. Bencardino, F.; Rizzuti, L.; Spadea, G.; Swamy, R.N. Stress–strain behavior of steel-fiber–reinforced concrete in compression. *J. Mater. Civ. Eng.* **2008**, *20*, 255–263. [CrossRef]
21. Bentur, A.; Mindess, S. *Fibre Reinforced Cementitious Composites*; Taylor and Francis: London, UK; New York, NY, USA, 2007.
22. Poveda, E.; Ruiz, G.; Cifuentes, H.; Yu, R.C.; Zhang, X. Influence of the fiber content on the compressive low-cycle fatigue behavior of self-compacting SFRC. *Int. J. Fatigue* **2017**, *101*, 9–17. [CrossRef]
23. Blason, S.; Poveda, E.; Ruiz, G.; Cifuentes, H.; Fernandez Canteli, A. Twofold normalization of the cyclic creep curve of plain and steel-fiber reinforced concrete and its application to predict fatigue failure. *Int. J. Fatigue* **2019**, *120*, 215–227. [CrossRef]
24. Neves, R. Modeling the Compressive Behaviour of Steel Fibre Reinforced Concrete. Master's Thesis, Instituto Superior Técnico, Lisbon, Portugal, 2000.
25. Rossi, P.; Harrouche, N. Mix design and mechanical behaviour of some steel fibre–reinforced concretes used in reinforced concrete structures. *Mater. Struct.* **1990**, *23*, 256–266. [CrossRef]
26. Rossi, P.; Harrouche, N. *Les Bétons de Fibres Métalliques*; Presses ENPC: Paris, France, 1998.

27. Nicolo, B.; De Pani, L.; Pozzo, E. Strain of concrete at peak compressive stress for a wide range of compressive strengths. *Mater. Struct.* **1994**, *27*, 206–210. [CrossRef]
28. Taerwe, L. Influence of steel fibres on strain–softening of high–strength concrete. *Mater. J.* **1992**, *88*, 54–60.
29. Rizzuti, L.; Bencardino, F. Effects of fibre volume fraction on the compressive and flexural experimental behavior of SFRC. *Contemp. Eng. Sci.* **2014**, *7*, 379–390. [CrossRef]
30. Bencardino, F.; Rizzuti, L.; Spadea, G. Experimental tests vs. theoretical modeling for FRC in compression. In Proceedings of the FraMCoS 6, Catania, Italy, 17–22 June 2007; pp. 159–166.
31. *ACI 544.4R-88 Design Considerations for Steel Fiber Reinforced Concrete*; ACI: Detroit, MI, USA, 1999.
32. Shah, S.P.; Stroeven, P.; Dalhuisen, D.; Van Stekelenburg, P. Complete stress–strain curves for steel fibre reinforced concrete in uniaxial tension and compression. In *Proc. Int. RYLEM Symp. Testing and Test Methods of Fibre Cement Composites*; Construction Press Ltd.: Lancaster, UK, 1978; pp. 399–408.
33. Fanella, D.A.; Naaman, A.E. stress–strain properties of fiber reinforced mortar in compression. *ACI J.* **1985**, *82*, 475–483.
34. Otter, D.; Naaman, A. Steel fibre reinforced concrete under static and cyclic compressive loading. In Proceedings of the 3rd International RILEM Symposium on Developments in Fiber Reinforced Cement and Concrete, RILEM Technical Committee 49-TFR, Lancaster, UK, 13–17 July 1986; Volume 1.
35. Song, P.S.; Hwang, S. Mechanical properties of high–strength steel-fiber–reinforced concrete. *Constr. Build. Mater.* **2004**, *18*, 669–673. [CrossRef]
36. Khaloo, A.; Kim, N. Mechanical properties of normal to high–strength steel fiber–reinforced concrete. *Cem. Concr. Aggreg.* **1996**, *18*, 92–97.
37. Marar, K.; Eren, Ö.; Celik, T. Relationship between impact energy and compression toughness energy of high–strength fiber– reinforced concrete. *Mater. Lett.* **2001**, *47*, 297–304. [CrossRef]
38. Thomas, J.; Ramaswamy, A. Mechanical properties of steel-fiber–reinforced concrete. *J. Mater. Civ. Eng.* **2007**, *19*, 385–392. [CrossRef]
39. Daniel, L.; Loukili, A. Behavior of high–strength fiber–reinforced concrete beams under cyclic loading. *ACI Struct. J.* **2002**, *99*, 248–256.
40. Hughes, B.P.; Fattuhi, N.I. Stress–strain curves for fiber reinforced concrete in compression. *Cem. Concr. Res.* **1977**, *7*, 173–183. [CrossRef]
41. Box, G.E.P.; Wilson, K.G. On the experimental attainment of optimum conditions. *J. R. Stat. Soc. B* **1951**, *13*, 1–45. [CrossRef]
42. Ruiz, G.; de la Rosa, Á.; Poveda, E. Model for the compressive stress–strain relationship of steel fiber–reinforced concrete for non–linear structural analysis. *Hormigón Acero* **2018**, *69* (Suppl. 1), 75–80. [CrossRef]
43. Behera, S.K.; Meena, H.; Chakraborty, S.; Meikap, B.C. Application of response surface methodology (rsm) for optimization of leaching parameters for ash reduction from low–grade coal. *Int. J. Min. Sci. Technol.* **2018**, *28*, 621–629. [CrossRef]
44. Montgomery, D.C. *Design and Analysis of Experiments*, 8th ed.; John Wiley and Sons: New York, NY, USA, 2014.
45. Myers, R.H.; Montgomery, D.C. *Response Surface Methodology, Process and Product Optimization Using Designed Experiments*; John Wiley and Sons: New York, NY, USA, 2002.
46. Grabiec, A.M.; Piasta, Z. Study on compatibility of cement–superplasticiser assisted by multicriteria statistical optimization. *J. Mater. Process. Technol.* **2004**, *152*, 197–203. [CrossRef]
47. Bayramov, F. Çimento Esasli Kompozit Malzemelerin Optimum Tasarimi. Ph.D. Thesis. Istanbul Teknik Universitesi, Istanbul, Turkey, 2004.
48. Nambiar, E.K.; Ramamurthy, K. Models relating mixture composition to the density and strength of foam concrete using response surface methodology. *Cem. Concr. Compos.* **2006**, *28*, 752–760. [CrossRef]
49. Maghsoud, A.; Amir, A.N.; Komeil, G. Response surface methodology and genetic algorithm in optimization of cement clinkering process. *J. Appl. Sci.* **2008**, *15*, 2732–2738.
50. Regulacion, R.E.; Oreta, A.W.C. Application of response surface methodology: optimum mix design of concrete with slag as coarse aggregate. In Proceedings of the 2013 World Congress on Advances in Structural Engineering and Mechanis (ASEM 13), Jeju, Korea, 8–12 September 2013.
51. Murali, T.M.; Kandasamy, S. Mix proportioning of high performance self–compacting concrete using response surface methodology. *J. Civ. Eng.* **2009**, *37*, 91–98. [CrossRef]

52. Li, Q.; Cai, L.; Fu, Y.; Wang, H.; Zou, Y. Fracture properties and response surface methodology model of alkali–slag concrete under freeze–thaw cycles. *Constr. Build. Mater.* **2015**, *93*, 620–626. [CrossRef]
53. Cho, T. Prediction of cyclic freeze–thaw damage in concrete structures based on response surface method. *Constr. Build. Mater.* **2007**, *21*, 2031–2040. [CrossRef]
54. Gupta, S.; Tripathi, R.K.; Mishra, R.K. Study of concrete having industrial waste as fine aggregate replacement and generation of model for prediction of compressive strength using response surface method. *Mater. Today* **2017**, *4*, 9727–9731. [CrossRef]
55. Timur Cihan, M.; Güner, A.; Yüzer, N. Response surfaces for compressive strength of concrete. *Constr. Build. Mater.* **2013**, *40*, 763–774. [CrossRef]
56. Kostic, S.; Vasovic, N.; Marinkovic, B. Robust optimization of concrete strength estimation using response surface methodology and monte carlo simulation. *Eng. Optim.* **2017**, *49*, 864–877. [CrossRef]
57. Bayramov, F.; Tasdemir, C.; Tasdemir, M.A. Optimisation of steel fibre reinforced concretes by means of statistical response surface method. *Cem. Concr. Compos.* **2004**, *26*, 665–675. [CrossRef]
58. Antony, J. *Design of Experiments for Engineers and Scientists*, 2nd ed.; Elsevier: Scotland, UK, 2014.
59. Box, G.E.; Hunter, J.S.; Hunter, W.G. *Estadística para Investigadores. Diseño, Innovación y Descubrimiento*, 2nd ed.; Reverté: Barcelona, Spain, 2008.
60. Gutiérrez, H.; de la Vara, R. *Análisis y Diseño de Experimentos*; McGraw–Hill: Álvaro Obregón, Mexico, 2003.
61. Vicente, M.L.; Girón, P.; Nieto, C.; Pérez, T. *Diseño de Experimentos. Soluciones con SAS y SPSS*; Pearson Educación: Madrid, Spain, 2005.
62. Mahalik, K.; Sahu, J.N.; Patwardhan, A.V.; Meikap, B.C. Statistical modeling and optimization of hydrolysis of urea to generate ammonia for flue gas conditioning. *J. Hazard. Mater.* **2010**, *10*, 603–610. [CrossRef] [PubMed]
63. Gunaraj, V.; Murugan, N. Application of response surface methodologies for predicting weld base quality in submerged arc welding of pipes. *J. Mater. Process. Technol.* **1999**, *88*, 266–275. [CrossRef]
64. Minitab 18 Statistical Software. 2018. Available online: www.minitab.com (accessed on 13 April 2018).
65. Sheather, S. *A Modern Approach to Regression with R*; Springer: New York, NY, USA, 2009.
66. EN 1992-1-1. *Eurocode 2: Design of Concrete Structures*; European Committee for Standardization–CEN: Brussels, Belgium, 2004.
67. EN 12390-3. *Testing Hardened Concrete—Part 3: Compressive Strength of Test Specimens*; European Committee for Standardization–CEN: Brussels, Belgium, 2009.
68. fib Bulletin 65/66. *Model Code 2010–Final Draft*; International Federation for Structural Concrete (fib): Lausanne, Switzerland, 2012.
69. Annex to PT1 prEN 1992-1-1 2018 D3. *Annex L – Steel Fibre Reinforced Concrete*; European Committee for Standardization–CEN: Brussels, Belgium, 31 October 2019.
70. Vicente, M.A.; Ruiz, G.; González, D.C.; Mínguez, J.; Tarifa, M.; Zhang, X.X. Effects of fiber orientation and content on the static and fatigue behavior of SFRC by using CT-Scan technology. *Int. J. Fatigue* **2019**, *128*, 105178. [CrossRef]
71. Ruiz, G.; de la Rosa, Á.; Poveda, E. Relationship between residual flexural strength and compression strength in steel-fiber reinforced concrete within the new Eurocode 2 regulatory framework. *Theor. Appl. Fract. Mech.* **2019**, *103*, 102310. [CrossRef]
72. Tiberti, G.; Germano, F.; Mudadu, A.; Plizzari, G.A. An overview of the flexural post–cracking behavior of steel-fiber reinforced concrete. *Struct. Concr.* **2018**, *19*, 695–718. [CrossRef]

© 2019 by the authors. Licensee MDPI, Basel, Switzerland. This article is an open access article distributed under the terms and conditions of the Creative Commons Attribution (CC BY) license (http://creativecommons.org/licenses/by/4.0/).